

Date of publication xxxx 00, 0000, date of current version xxxx 00, 0000.

Digital Object Identifier 10.1109/ACCESS.2024.0429000

HiFiSeg: High-Frequency Information Enhanced Polyp Segmentation with Global-Local Vision Transformer

JINGJING REN, XIAOYONG ZHANG, and LINA ZHANG.

Department of Intelligence and Information Engineering, Taiyuan University, Taiyuan 030032, CHINA (e-mail: renjingjing@tyu.edu.cn)

Corresponding author: JINGJING REN (e-mail: 2014010020@tyu.edu.cn).

This work was supported in part by the Science and Technology Innovation Program of Higher Education Institutions in Shanxi Province 2024L386

ABSTRACT Numerous studies have demonstrated the strong performance of vision transformer (ViT)-based methods across various computer vision tasks. However, ViT models often struggle to effectively capture high-frequency components in images, which are crucial for detecting small targets and preserving edge details, especially in complex scenarios. This limitation is particularly challenging in colon polyp segmentation, where polyps exhibit significant variability in structure, texture, and shape. High-frequency information, such as boundary details, is essential for achieving precise semantic segmentation in this context. To address these challenges, we propose HiFiSeg, a novel network for colon polyp segmentation that enhances high-frequency information processing through a global-local vision transformer framework. HiFiSeg leverages the pyramid vision transformer (PVT) as its encoder and introduces two key modules: the global-local interaction module (GLIM) and the selective aggregation module (SAM). GLIM employs a parallel structure to fuse global and local information at multiple scales, effectively capturing fine-grained features. SAM selectively integrates boundary details from low-level features with semantic information from high-level features, significantly improving the model's ability to accurately detect and segment polyps. Extensive experiments on five widely recognized benchmark datasets demonstrate the effectiveness of HiFiSeg for polyp segmentation. Notably, the mDice scores on the challenging CVC-ColonDB and ETIS datasets reached 0.826 and 0.822, respectively, underscoring the superior performance of HiFiSeg in handling the specific complexities of this task.

INDEX TERMS polyp segmentation, colonoscopy, deep learning, pyramid vision transformer.

I. INTRODUCTION

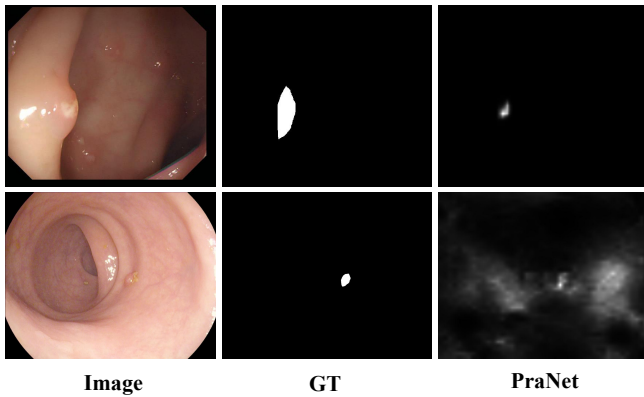
POLYPS are abnormal growths in the colon and rectum that protrude from the intestinal mucosa. Colorectal cancer frequently arises from colonic polyps, especially adenomatous ones, making early detection and removal critical for preventing cancer progression. Colonoscopy is widely regarded as the gold standard for detecting colorectal lesions [1]. However, the manual annotation of polyps during colonoscopy is both time-consuming and prone to human error, underscoring the need for automated and accurate image segmentation methods to assist in diagnosis.

Deep learning algorithms, particularly CNNs, have achieved significant success in medical image applications such as cardiac, skin lesion, and polyp segmentation [2]. Fully convolutional networks (FCNs), including models like UNet [3], SegNet [4], and DeepLab [5], have become the

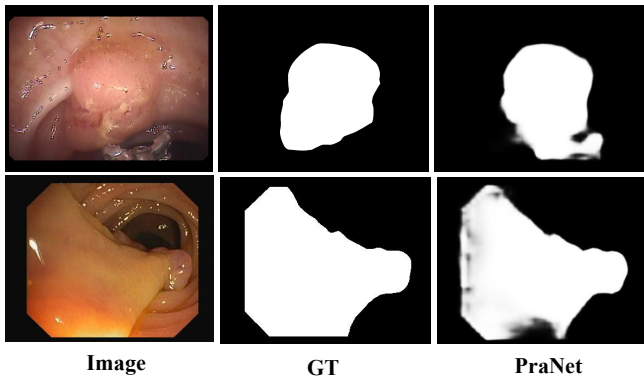
dominant approaches in this domain. However, due to the limited receptive fields of CNNs, these methods struggle to capture long-range dependencies and global context, which are essential for accurately representing shape and structural information in medical image segmentation.

The transformer [6] architecture, with its multi-head self-attention (MHSA) mechanism, excels at capturing complex spatial transformations and long-range dependencies. While it has seen tremendous success in natural language processing (NLP), its adaptation to vision tasks through the vision transformer (ViT) [7] was aimed at overcoming the limitations of CNNs in image recognition. However, despite Transformers' ability to model global dependencies, they struggle with capturing image locality and maintaining translational invariance, which is critical for accurately segmenting small targets and boundaries. To address this challenge, recent

arXiv:2410.02528v2 [cs.CV] 10 Oct 2024



(a) Small targets with strong camouflage are difficult to segment.



(b) Fuzzy positioning of object boundaries

FIGURE 1. Examples of segmentation of the PraNet model for different challenge cases.

works have proposed hybrid architectures [8]–[10] that combine the strengths of both Transformers and CNNs, such as TransUnet [11], HiFormer [12], and LeViT-Unet [13]. These models aim to leverage the locality of CNNs with the global context captured by Transformers, enabling them to encode both local and global features for medical image segmentation. While these hybrid models have shown improved performance, they still face limitations, particularly in capturing fine-grained details. This shortcoming affects the accurate identification of small targets and boundary localization, hindering the model’s ability to generalize effectively in medical image segmentation. As illustrated in Figure 1, the PraNet model highlights some of the persistent challenges in polyp segmentation, underscoring the need for better methods to address these issues.

Inspired by multiscale and multilevel feature modeling approaches [14]–[17], we propose a high-frequency information-enhanced polyp segmentation framework, termed **HiFiSeg**. The main components of HiFiSeg include the pyramid vision transformer (PVT), the global-local interaction module (GLIM), and the selective aggregation module (SAM). PVT, a lightweight hierarchical Transformer, serves as the encoder to capture multiscale features efficiently. GLIM employs parallel convolutional kernels and pooling

operations of varying sizes to aggregate global and local information, allowing the extraction of fine-grained features. This is particularly advantageous for localizing small targets. To reduce computational complexity, GLIM uses grouped channels with depthwise separable convolution. SAM refines boundary features by leveraging high-level semantic information to guide the selective refinement of low-level details.

In summary, our contributions are as follows:

- We propose **HiFiSeg**, a novel framework for colon polyp segmentation. HiFiSeg utilizes the Pyramid Vision Transformer as an encoder to capture more robust features than CNN-based methods.
- We design two key modules, **GLIM** and **SAM**, to enhance the framework. GLIM improves segmentation performance for small targets by extracting multiscale local features, while SAM addresses boundary ambiguity by selectively fusing low-level boundary details with high-level semantic information.
- We evaluate HiFiSeg on five standard benchmark datasets for polyp segmentation, including Kvasir [18], CVC-ClinicDB [19], CVC-300 [20], CVC-ColonDB [21], and ETIS [22]. On the challenging CVC-ColonDB and ETIS datasets, HiFiSeg achieves mDice scores of 0.826 and 0.822, respectively, surpassing existing state-of-the-art methods.

II. RELATED WORK

A. CONVOLUTIONAL NEURAL NETWORKS

CNNs are deep learning models specifically designed for processing image data, excelling in feature extraction capabilities, and are widely used in computer vision tasks. In recent years, CNN-based structures represented by the UNet architecture have made significant progress in medical image segmentation. UNet consists of a symmetric encoder and decoder, with skip connections that transfer features from the encoder to the decoder, combining low-level features and high-level semantic information to achieve high-precision segmentation. Many works have made improvements based on the UNet architecture, such as UNet++ [23], ResUNet++ [24] and DoubleUnet [25].

Unlike the UNet-based methods, PolypNet [26] proposed a dual-tree wavelet pooling CNN with a local gradient-weighted embedding level set, significantly reducing the false positive rate, significantly reducing the false positive rate. Caranet [27] proposed a context axial reserve attention network to improve the segmentation performance on small objects. PraNet [28] generates a global map based on high-level features aggregated by the parallel partial decoder and employs the reverse attention module to mine boundary cues, effectively correcting any misaligned predictions, thereby improving segmentation accuracy.

B. VISION TRANSFORMER

Transformer [6], proposed by Vaswani et al., uses multi-head self-attention to capture long-range dependencies. Initially designed for natural language tasks like translation, Transformers are now widely used in image processing and

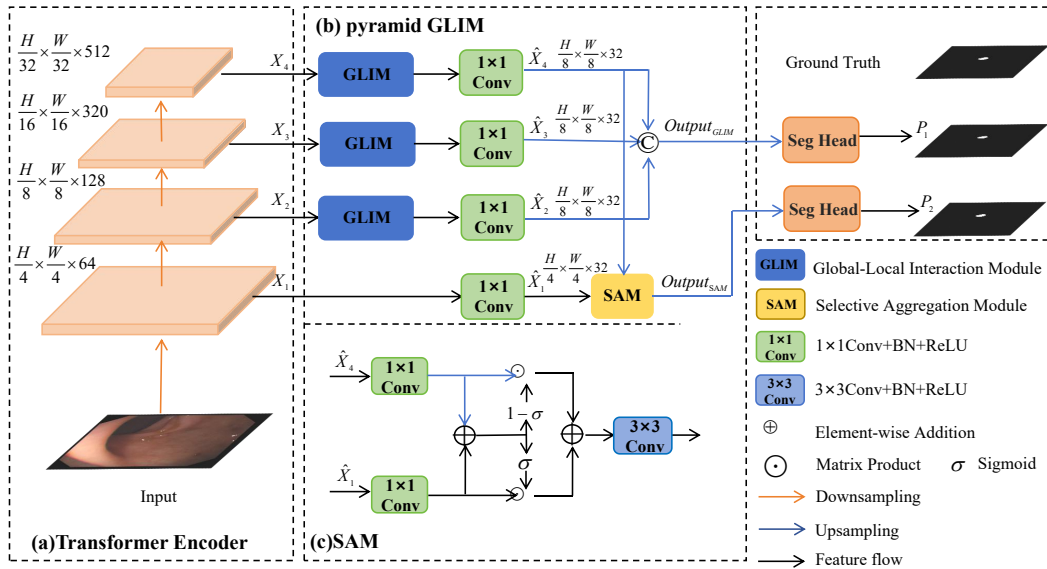


FIGURE 2. The overall architecture of HiFiSeg network. The entire model contains three components: (a) pyramid vision transformer (PVT) as encoder; (b) pyramid global-local interaction module (GLIM) for fusing multi-level features; (c) selective aggregation module (SAM) for integrating the high- and low-level features selectively for the final output.

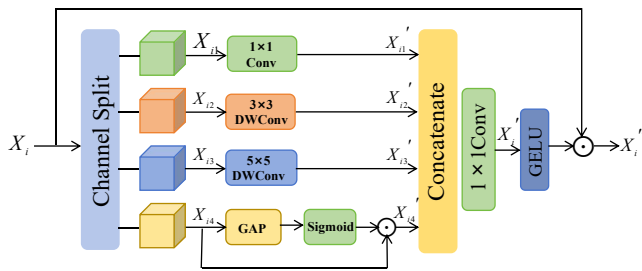


FIGURE 3. Details of the introduced global-local interaction module (GLIM). It consists of three convolutional branches and a global average pooling branch.

speech recognition due to their parallel processing and global context modeling. Vision transformer (ViT) [7] was the first pure Transformer for image classification, processing images as fixed-size patches. Subsequent models like Swin Transformer [29], PVT [14], and Segformer [30] introduced pyramid structures for improved vision tasks. Meanwhile, diffusion models [31]–[34] have become popular for iteratively refining images through noise reduction. When combined with Transformers, they enhance feature extraction and segmentation, improving performance in tasks like medical image segmentation and object detection.

In medical image segmentation, hybrid architectures combining Transformers and CNNs have shown promise. Transfuse [35] integrates Transformers and CNNs to capture global and local features, while TransUNet [11] uses Transformers as encoders and U-Net to refine local details. Polyp-PVT [36] leverages PVT as an encoder with a graph-based similarity aggregation module. ColonFormer [37] models global semantic relations and refines polyp boundaries, while DuAT [38] introduces dual-aggregate Transformers to bal-

ance large and small target detection and enhance boundary precision.

III. PROPOSED METHOD

A. OVERVIEW

As shown in Figure 2, our proposed network HiFiSeg consists of a pyramid vision transformer (PVT) encoder, global-local interaction module (GLIM), and selective aggregation module (SAM). The PVT encoder is employed to extract multi-scale hierarchical features from the input image $X \in \mathbb{R}^{H \times W \times 3}$, capturing both fine-grained local details and broad semantic information. Specifically, the PVT backbone yields four pyramid features $X_i \in \mathbb{R}^{\frac{H}{2^{i+1}} \times \frac{W}{2^{i+1}} \times C_i}$, where $i \in \{1, 2, 3, 4\}$ and $C_i \in \{64, 128, 320, 512\}$. The high-level features $\{X_i | i \in (2, 3, 4)\}$ are fed into the GLIM module to extract local multiscale features. The outputs of the GLIM module are then concatenated to produce the fused global-local multiscale feature $Output_{GLIM}$. The low-level feature X_1 is selectively aggregated with the high-level feature X_4 through the SAM module to obtain the enhanced edge feature $Output_{SAM}$. Finally, $Output_{GLIM}$ and $Output_{SAM}$ are fed into the segmentation heads to obtain the predicted results P_1 and P_2 , respectively.

B. TRANSFORMER ENCODER

Some recent studies have demonstrated that pyramid structures, through the integration of multi-scale contextual information, can substantially improve the accuracy and efficiency of image segmentation. Our model uses the pyramid vision transformer (PVT) proposed in [46] as the encoder backbone to extract more robust features for polyp segmentation. PVT is the first pure Transformer backbone designed for various pixel-level dense prediction tasks. In

polyp segmentation, PVT generates four multi-scale feature maps $\{X_i | i \in (1, 2, 3, 4)\}$. Among these feature maps, X_1 gives detailed information about the polyps, while X_2 , X_3 , and X_4 provide high-level features.

C. GLOBAL-LOCAL INTERACTION MODULE

In medical image segmentation, the context and background often occupy a much larger area than the segmentation target itself. Consequently, capturing information across different scales is essential for accurately segmenting small targets. Instead of presenting multi-scale features in a layer-by-layer fashion, GLIM aggregates global and local features at a specific high-level, achieving multi-scale feature representation at a granular level, reducing errors in high-level features.

The detailed architecture of our proposed GLIM is depicted in Figure 3, consisting of three convolution branches and one pooling branch. To balance accuracy and computational resources, we evenly divide the channels into four groups, applying depthwise separable convolution for each. After splitting the input features $\{X_i | i \in \{2, 3, 4\}\}$ into four components $X_{i1}, X_{i2}, X_{i3}, X_{i4}$, they are fed into feature generation units at different scales. Given the input feature X_i , this procedure can be formulated as:

$$\begin{aligned} X_{i1}, X_{i2}, X_{i3}, X_{i4} &= \text{Split}(X) \\ X'_{i1} &= \text{Conv}_{1 \times 1}(X_{i1}) \\ X'_{i2} &= \text{DWConv}_{3 \times 3}(X_{i2}) \\ X'_{i3} &= \text{DWConv}_{5 \times 5}(X_{i3}) \\ X'_{i4} &= \text{Sigmoid}(\text{GAP}(X_{i4})) \odot (X_{i4}), \end{aligned} \quad (1)$$

where $\text{Split}(\cdot)$ denotes the channel separation operation, $\text{Conv}_{1 \times 1}(\cdot)$ represents 1×1 convolution, $\text{DWConv}_{3 \times 3}(\cdot)$ refers to 3×3 depth-wise convolution, $\text{DWConv}_{5 \times 5}(\cdot)$ refers to 5×5 depth-wise convolution, GAP stands for global average pooling, Sigmoid refers to the Sigmoid activation function, and \odot is the element-wise product. The convolution branches employ kernels of varying sizes to extract features at different scales of the image, while the pooling branch uses global average pooling to aggregate global information. These feature maps $\{X'_{i1}, X'_{i2}, X'_{i3}, X'_{i4}\}$ are then concatenated along the channel dimension, and a 1×1 convolution is applied to aggregate both global and local information, resulting in a rich feature representation X'_i . This process can be expressed as:

$$X'_i = \text{Conv}_{1 \times 1}(\text{Concat}([X'_{i1}, X'_{i2}, X'_{i3}, X'_{i4}])), \quad (2)$$

where $\text{Concat}(\cdot)$ denotes a concatenation operation, while $\text{Conv}_{1 \times 1}(\cdot)$ refers to a 1×1 convolution. To enhance feature selection, we apply the GELU activation function to the feature X'_i to generate the attention feature map, and then modulate the input feature X through element-wise multiplication. It can be formulated as:

$$X''_i = \text{GELU}(X'_i) \odot X_i, \quad (3)$$

where GELU refers to the GELU activation function, and \odot is the element-wise product.

D. SELECTIVE AGGREGATION MODULE

Shallow features contain rich spatial information, while deep features contain more semantic information. The effective combination of these two is crucial for improving the accuracy of the model. In order to enhance the guidance of shallow detail features by deep semantic features, we propose the selective aggregation module (SAM), as shown in Figure 1(c). Unlike previous fusion methods that directly add the provided feature maps, SAM selectively aggregates the features. First, the shallow feature \hat{X}_1 and deep feature \hat{X}_4 are individually processed through 1×1 convolutions followed by sigmoid activations to produce the attention weight σ . The output of the Sigmoid function could be represented as:

$$\sigma = \text{Sigmoid}(C_{1 \times 1}(\hat{X}_1) \oplus C_{1 \times 1}(\hat{X}_4)). \quad (4)$$

If σ is high, the model assigns greater trust to the shallow feature, and vice versa. The output of the SAM can be written as:

$$\text{Output}_{\text{SAM}} = \sigma \hat{X}_1 \oplus (1 - \sigma) \hat{X}_4. \quad (5)$$

E. LOSS FUNCTION

We use weighted binary cross-entropy (BCE) loss and the weighted intersection over union (IoU) loss for supervision. Our loss function can be formulated as Eqn. 6:

$$\begin{aligned} L_{\text{total}} &= L(P_1, G) + L(P_2, G) \\ L(P_1, G) &= \lambda_1 L_{\text{BCE}}^w(P_1, G) + \lambda_2 L_{\text{IoU}}^w(P_1, G) \\ L(P_2, G) &= \lambda_1 L_{\text{BCE}}^w(P_2, G) + \lambda_2 L_{\text{IoU}}^w(P_2, G), \end{aligned} \quad (6)$$

where P_1, P_2 are the outputs and G is the ground truth, λ_1 and λ_2 are the weighting coefficients, $L_{\text{BCE}}^w(\cdot)$ and $L_{\text{IoU}}^w(\cdot)$ are the weighted BCE and weighted IoU.

IV. EXPERIMENT AND ANALYSIS

To validate the proposed HiFiSeg method's superiority, it is compared with multiple state-of-the-art approaches on five popular datasets for polyp segmentation, namely, Kvasir [18], CVC-ClinicDB [19], CVC-300 [20], CVC-ColonDB [21], ETIS [22].

A. DATASETS

We used five challenging public datasets for the polyp segmentation task, including Kvasir [18], CVC-ClinicDB [19], CVC-300 [20], CVC-ColonDB [21], and ETIS [22], to validate the learning and generalization capabilities of our model. Details for each dataset are as follows:

Kvasir dataset: The dataset consists of 1000 images with different resolutions from 720×576 to 1920×1072 pixels.

CVC-ClinicDB dataset: The dataset contains 612 polyp images which are extracted from 29 different endoscopic video clips. The resolution of images is 384×288 .

CVC-300 dataset: The dataset consists of 60 polyp images and the resolution of the images is 574×500 .

CVC-ColonDB dataset: The dataset consists of 380 polyp images and the resolution of the images is 570×500 .

ETIS dataset: The dataset consists of 196 polyp images and the resolution of the images is 1225×966 .

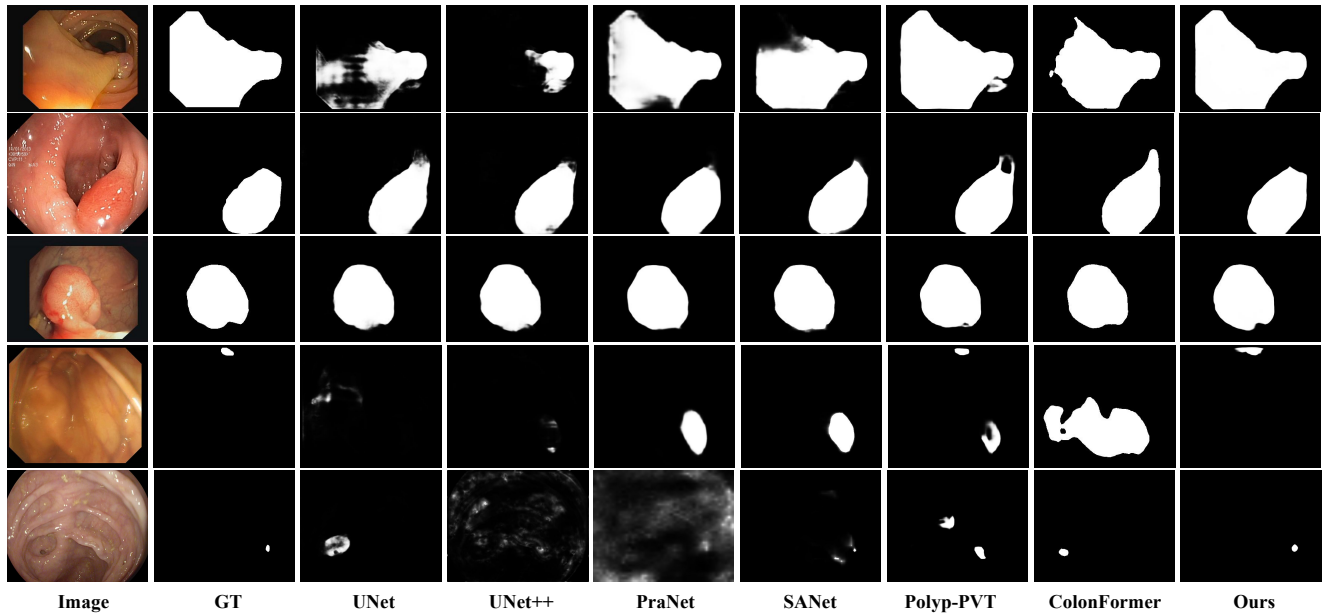


FIGURE 4. Qualitative results comparison of different models.

TABLE 1. Quantitative Evaluation of the Learning Ability of Our Proposed HiFiSeg and Other Methods on the Kvasir and CVC-ClinicDB Datasets.

Methods	Kvasir			CVC-ClinicDB		
	mDice	mIoU	MAE	mDice	mIoU	MAE
U-Net [3]	0.818	0.746	0.055	0.823	0.755	0.055
UNet++ [23]	0.821	0.743	0.048	0.794	0.729	0.022
Pranet [28]	0.898	0.840	0.030	0.899	0.849	0.009
SANet [39]	0.904	0.847	0.028	0.916	0.859	0.012
TransUnet [11]	0.913	0.857	0.028	0.935	0.887	0.008
SSFormer [40]	0.926	0.874	0.023	0.927	0.876	0.009
Polyp-PVT [36]	0.917	0.864	0.023	0.937	0.889	0.006
ColonFormer-S [37]	0.927	0.877	0.021	0.932	0.883	0.008
HiFiSeg(Ours)	0.933	0.886	0.018	0.942	0.897	0.006

B. EVALUATION METRICS

We employ three widely-used metrics in the field of medical image segmentation, i.e., mean Dice (mDice), mean IoU (mIoU) and mean absolute error (MAE) to evaluate the model performances. Mean Dice and IoU are widely utilized metrics that primarily focus on assessing the internal consistency of segmentation results. MAE, on the other hand, measures the pixel-level accuracy by calculating the average absolute error between the predicted and actual values.

C. IMPLEMENTATION DETAILS

We randomly split the images from Kvasir and CVC-ClinicDB into 80% for training and 20% for testing. And test on CVC-300, CVC-ColonDB and ETIS datasets. Due to the uneven resolution of the images, we resized them to 352×352 resolution.

We implement the HiFiSeg using the PyTorch framework,

utilizing an NVIDIA RTX 3090 GPU. To enhance the model's robustness concerning varying image sizes, the training images are scaled by factors of 0.75, 1, and 1.25 [37], respectively, before being fed into the model for learning. PVT encoder uses the same parameters as pvt_v2_b2 [41]. The model is trained end-to-end using the AdamW [42] optimizer, with the learning rate and weight decay set to $1e-4$. The batch size is configured to 16.

D. COMPARISON WITH STATE-OF-THE-ART METHODS

1) Learning Ability

We first evaluate the learning ability of the proposed model HiFiSeg on the training datasets Kvasir and ClinicDB. As shown in Table 1, we compare our proposed HiFiSeg with recently published and classical models for polyp segmentation, including CNN-based models such as UNet [3], UNet++ [23], PraNet [28], and SANet [39], as well as Transformer-based

TABLE 2. Quantitative Evaluation of the Generalization Ability of Our Proposed HiFiSeg and Other Methods on the CVC-300, CVC-ColonDB and ETIS Datasets.

Methods	CVC-300			CVC-ColonDB			ETIS		
	mDice	mIoU	MAE	mDice	mIoU	MAE	mDice	mIoU	MAE
UNet [3]	0.710	0.627	0.022	0.512	0.444	0.061	0.398	0.335	0.036
UNet++ [23]	0.707	0.624	0.018	0.794	0.729	0.022	0.401	0.344	0.035
Pranet [28]	0.851	0.797	0.010	0.712	0.640	0.043	0.628	0.567	0.031
SANet [39]	0.888	0.815	0.008	0.753	0.670	0.043	0.750	0.654	0.015
TransUnet [11]	0.893	0.660	0.009	0.781	0.699	0.036	0.731	0.824	0.021
SSFormer [40]	0.887	0.821	0.007	0.772	0.697	0.036	0.767	0.698	0.016
Polyp-PVT [36]	0.900	0.833	0.007	0.808	0.727	0.031	0.787	0.706	0.013
ColonFormer-S [37]	0.894	0.826	0.008	0.811	0.730	0.027	0.789	0.711	0.013
HiFiSeg (Ours)	0.905	0.839	0.006	0.826	0.749	0.028	0.822	0.743	0.012

TABLE 3. QUANTITATIVE RESULTS FOR ABLATION STUDIES.

Methods	Kvasir		CVC-ClinicDB		CVC-300		CVC-ColonDB		ETIS	
	mDice	mIoU	mDice	mIoU	mDice	mIoU	mDice	mIoU	mDice	mIoU
Baseline	0.910	0.856	0.903	0.847	0.869	0.792	0.796	0.707	0.759	0.668
w/o GLIM	0.924	0.878	0.937	0.892	0.892	0.828	0.813	0.734	0.798	0.725
w/o SAM	0.918	0.871	0.924	0.879	0.896	0.833	0.798	0.721	0.801	0.729
w/o Conv	0.923	0.877	0.931	0.883	0.886	0.816	0.808	0.732	0.788	0.710
w/o GAP	0.928	0.878	0.934	0.884	0.899	0.833	0.811	0.726	0.781	0.704
HiFiSeg	0.933	0.886	0.942	0.897	0.905	0.839	0.826	0.749	0.822	0.743

models like TransUnet [11], SSFormer [40], Polyp-PVT [36], and ColonFormer [37]. These results demonstrate the effectiveness of our model in accurately segmenting polyps. Specifically, the HiFiSeg model has a mDice value of 0.933 and a mIoU value of 0.876 on Kvasir dataset, which are 0.6% and 0.9% higher than the best performing model, ColonFormer, respectively. For CVC-ClinicDB dataset, the HiFiSeg model has a mDice value of 0.942 and a mIoU value of 0.897, which are 0.6% and 0.8% higher than the best performing model, Polyp-PVT, respectively.

2) Generalization Capabilities

To further evaluate our model's generalization performance, we test HiFiSeg on three unseen datasets: CVC-300, CVC-ColonDB, and ETIS. These datasets originate from different medical centers, each presenting unique challenges and characteristics. As seen in Table 2, on three unseen datasets, our model outperforms peer models across all metrics, demonstrating strong generalization performance. On CVC-300 dataset, HiFiSeg achieves mDice of 0.905 and mIoU of 0.839, outperforming the second-best model, Polyp-PVT, by 0.5% and 0.6%, respectively. On CVC-ColonDB dataset, our model's mDice and mIoU scores are 1.5% and 1.9% higher than those of ColonFormer, respectively. Moreover, HiFiSeg achieves mDice of 0.822 and mIoU of 0.743 on ETIS dataset, which are 3.3% and 3.2% higher than the second-best model ColonFormer.

3) Visual Results

Figure 4 presents the visualization results of our model alongside the comparison models, providing a qualitative assessment of their performance. As shown in Figure 4, our model produces significantly fewer incorrectly predicted pixels in the segmentation results compared to other models. It accurately identifies colonic tissues and polyps, efficiently captures the boundaries of tiny polyps and target objects, and maintains stable recognition and segmentation capabilities across various imaging conditions. As seen in the first three rows of Figure 4, HiFiSeg accurately captures the boundaries and fine details of the target object, whereas the other methods fail to clearly detect the boundaries. In rows 4 and 5, our method demonstrates superior ability in identifying small targets and produces more accurate segmentation predictions.

E. ABLATION STUDIES AND ANALYSIS

We use PVTv2 as our baseline (Bas.) and evaluate module effectiveness by removing components from the complete GLIM. The training, testing, and hyperparameter settings are the same as mentioned in Sec. III-C. The results are shown in Table 3.

Effectiveness of GLIM. To evaluate the effectiveness of GLIM, we trained a version of the model: "HiFiSeg (w/o GLIM)." As shown in Table 3, compared to the standard HiFiSeg network, the performance of HiFiSeg (w/o GLIM) is reduced across all five datasets. This is particularly noticeable

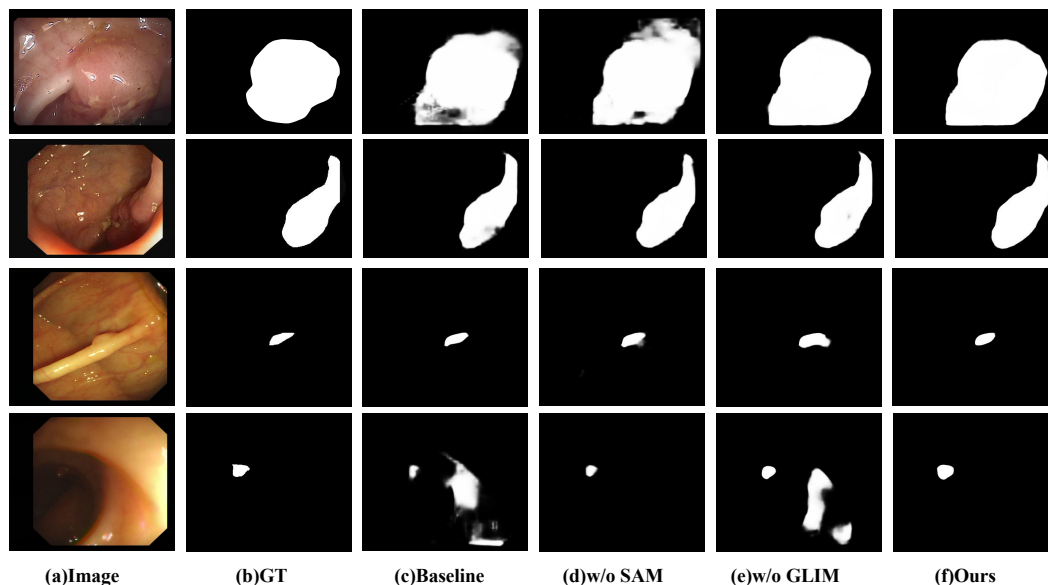


FIGURE 5. Visualization of the ablation study results.

on ETIS dataset, where the mDice drops from 0.822 to 0.798 and the mIoU decreases from 0.743 to 0.725. As shown in the visualization results in Figure 5, the HiFiSeg (w/o GLIM) model struggles to effectively distinguish between polyps and colon tissues and has difficulty accurately localizing targets, particularly small ones. In contrast, the HiFiSeg model, with the inclusion of the GLIM module, significantly improves the accuracy of target localization and small target detection due to the aggregation of local and global features.

Effectiveness of SAM. To evaluate the effectiveness of SAM, we trained a version of the model: "HiFiSeg (w/o SAM)." As shown in Table 3, compared to HiFiSeg(w/o SAM), HiFiSeg shows a substantial improvement in performance on all five datasets. Specifically, the mdice on CVC-ColonDB dataset is improved from 0.798 to 0.826 and the mIoU is mentioned from 0.721 to 0.749, both of which are improved by 2.8%. The visualization results in Figure 5 show that SAM enables more accurate boundary extraction by effectively combining local pixel information with global semantic cues.

Effectiveness of GLIM module components. The GLIM consists of three convolution branches and one global average pooling(GAP) branch. The convolutional branches extract local features at multiple scales using convolutional kernels of varying sizes, while the global average pooling branch captures global information by spatially averaging the entire feature map, thereby better capturing the overall semantic context. To verify the effectiveness of the convolutional branches, we removed it from GLIM, resulting in HiFiSeg (w/o Conv). As shown in Table 3, compared to the original HiFiSeg, the performance of the modified model drops significantly due to the lack of rich local representations, particularly on the ETIS dataset, where mDice and mIoU decrease by 3.4% and 3.3%,

respectively. To verify the effectiveness of GAP, it is replaced with a 7×7 convolution, resulting in the model HiFiSeg (w/o GAP). As shown in Table 3, the lack of global semantic information leads to a performance decline across all datasets, particularly on the ETIS dataset, where mDice and mIoU drop by 4.1% and 3.9%, respectively.

V. CONCLUSION

In this paper, we proposed HiFiSeg network to address the challenges in colon polyp image segmentation, such as fine-grained target localization and boundary feature enhancement. Specifically, the GLIM fused global and local features by extracting multi-scale features in parallel, which facilitated the localization of targets of varying sizes. The SAM selectively combined semantic features with detailed features to alleviate the issue of unclear boundaries, further enhancing performance. Experimental results on five representative colon polyp datasets demonstrated that the HiFiSeg algorithm possessed strong learning and generalization capabilities, outperforming other competing methods. In future work, we plan to explore lightweight architectures to reduce model complexity, thereby extending its applicability to a wider range of medical image segmentation tasks.

REFERENCES

- [1] P. Favoriti, G. Carbone, M. Greco, F. Pirozzi, R. E. M. Pirozzi, and F. Corcione, "Worldwide burden of colorectal cancer: a review," *Updates in Surgery*, vol. 68, no. 1, pp. 7–11, 2016.
- [2] K. Yan, F. Shen, and Z. Li, "Enhancing landslide segmentation with guide attention mechanism and fast fourier transformer," in *International Conference on Intelligent Computing*. Springer, 2024, pp. 296–307.
- [3] O. Ronneberger, P. Fischer, and T. Brox, "U-net: Convolutional networks for biomedical image segmentation," in *Medical image computing and computer-assisted intervention—MICCAI 2015: 18th international conference, Munich, Germany, October 5-9, 2015, proceedings, part III 18*. Springer, 2015, pp. 234–241.

- [4] V. Badrinarayanan, A. Kendall, and R. Cipolla, "Segnet: A deep convolutional encoder-decoder architecture for image segmentation," *IEEE transactions on pattern analysis and machine intelligence*, vol. 39, no. 12, pp. 2481–2495, 2017.
- [5] L.-C. Chen, G. Papandreou, I. Kokkinos, K. Murphy, and A. L. Yuille, "DeepLab: Semantic image segmentation with deep convolutional nets, atrous convolution, and fully connected crfs," *IEEE transactions on pattern analysis and machine intelligence*, vol. 40, no. 4, pp. 834–848, 2017.
- [6] A. Vaswani, N. Shazeer, N. Parmar, J. Uszkoreit, L. Jones, A. N. Gomez, Ł. Kaiser, and I. Polosukhin, "Attention is all you need," *Advances in neural information processing systems*, vol. 30, 2017.
- [7] A. Dosovitskiy, L. Beyer, A. Kolesnikov, D. Weissenborn, X. Zhai, T. Unterthiner, M. Dehghani, M. Minderer, G. Heigold, S. Gelly *et al.*, "An image is worth 16x16 words: Transformers for image recognition at scale," *arXiv preprint arXiv:2010.11929*, 2020.
- [8] F. Shen, Y. Xie, J. Zhu, X. Zhu, and H. Zeng, "Git: Graph interactive transformer for vehicle re-identification," *IEEE Transactions on Image Processing*, vol. 32, pp. 1039–1051, 2023.
- [9] F. Shen, X. Shu, X. Du, and J. Tang, "Pedestrian-specific bipartite-aware similarity learning for text-based person retrieval," in *Proceedings of the 31st ACM International Conference on Multimedia*, 2023, pp. 8922–8931.
- [10] F. Shen, X. Du, L. Zhang, X. Shu, and J. Tang, "Triplet contrastive representation learning for unsupervised vehicle re-identification," *arXiv preprint arXiv:2301.09498*, 2023.
- [11] J. Chen, Y. Lu, Q. Yu, X. Luo, E. Adeli, Y. Wang, L. Lu, A. L. Yuille, and Y. Zhou, "Transunet: Transformers make strong encoders for medical image segmentation," *arXiv preprint arXiv:2102.04306*, 2021.
- [12] M. Heidari, A. Kazerouni, M. Soltany, R. Azad, E. K. Aghdam, J. Cohen-Adad, and D. Merhof, "Hiformer: Hierarchical multi-scale representations using transformers for medical image segmentation," in *Proceedings of the IEEE/CVF winter conference on applications of computer vision*, 2023, pp. 6202–6212.
- [13] G. Xu, X. Zhang, X. He, and X. Wu, "Levit-unet: Make faster encoders with transformer for medical image segmentation," in *Chinese Conference on Pattern Recognition and Computer Vision (PRCV)*. Springer, 2023, pp. 42–53.
- [14] W. Wang, E. Xie, X. Li, D.-P. Fan, K. Song, D. Liang, T. Lu, P. Luo, and L. Shao, "Pyramid vision transformer: A versatile backbone for dense prediction without convolutions," in *Proceedings of the IEEE/CVF international conference on computer vision*, 2021, pp. 568–578.
- [15] G. Gao, Y. Guo, L. Zhou, L. Li, and G. Shi, "Res2net-based multi-scale and multi-attention model for traffic scene image classification," *PLoS One*, vol. 19, no. 5, p. e0300017, 2024.
- [16] W. Zhang, J. Li, U. A. Bhatti, J. Liu, J. Zheng, and Y.-W. Chen, "Robust multi-watermarking algorithm for medical images based on googlenet and henon map," *Comput. Mater. Contin.*, vol. 75, pp. 565–586, 2023.
- [17] H. Wang, P. Cao, J. Yang, and O. Zaiane, "Mca-unet: multi-scale cross co-attentional u-net for automatic medical image segmentation," *Health information science and systems*, vol. 11, no. 1, p. 10, 2023.
- [18] D. Jha, P. H. Smedsrud, M. A. Riegler, P. Halvorsen, T. De Lange, D. Johansen, and H. D. Johansen, "Kvasir-seg: A segmented polyp dataset," in *MultiMedia modeling: 26th international conference, MMM 2020, Daejeon, South Korea, January 5–8, 2020, proceedings, part II 26*. Springer, 2020, pp. 451–462.
- [19] J. Bernal, F. J. Sánchez, G. Fernández-Esparrach, D. Gil, C. Rodríguez, and F. Vilariño, "Wm-dova maps for accurate polyp highlighting in colonoscopy: Validation vs. saliency maps from physicians," *Computerized medical imaging and graphics*, vol. 43, pp. 99–111, 2015.
- [20] D. Vázquez, J. Bernal, F. J. Sánchez, G. Fernández-Esparrach, A. M. López, A. Romero, M. Drozdal, and A. Courville, "A benchmark for endoluminal scene segmentation of colonoscopy images," *Journal of healthcare engineering*, vol. 2017, no. 1, p. 4037190, 2017.
- [21] N. Tajbakhsh, S. R. Gurudu, and J. Liang, "Automated polyp detection in colonoscopy videos using shape and context information," *IEEE transactions on medical imaging*, vol. 35, no. 2, pp. 630–644, 2015.
- [22] J. Silva, A. Hístace, O. Romain, X. Dray, and B. Granado, "Toward embedded detection of polyps in wce images for early diagnosis of colorectal cancer," *International journal of computer assisted radiology and surgery*, vol. 9, pp. 283–293, 2014.
- [23] Z. Zhou, M. M. Rahman Siddiquee, N. Tajbakhsh, and J. Liang, "Unet++: A nested u-net architecture for medical image segmentation," in *Deep Learning in Medical Image Analysis and Multimodal Learning for Clinical Decision Support: 4th International Workshop, DLMIA 2018, and 8th International Workshop, ML-CDS 2018, Held in Conjunction with MICCAI 2018, Granada, Spain, September 20, 2018, Proceedings 4*. Springer, 2018, pp. 3–11.
- [24] D. Jha, P. H. Smedsrud, M. A. Riegler, D. Johansen, T. De Lange, P. Halvorsen, and H. D. Johansen, "Resunet++: An advanced architecture for medical image segmentation," in *2019 IEEE international symposium on multimedia (ISM)*. IEEE, 2019, pp. 225–2255.
- [25] D. Jha, M. A. Riegler, D. Johansen, P. Halvorsen, and H. D. Johansen, "Doubleu-net: A deep convolutional neural network for medical image segmentation," in *2020 IEEE 33rd International symposium on computer-based medical systems (CBMS)*. IEEE, 2020, pp. 558–564.
- [26] D. Banik, K. Roy, D. Bhattacharjee, M. Nasipuri, and O. Krejcar, "Polyp-net: A multimodal fusion network for polyp segmentation," *IEEE Transactions on Instrumentation and Measurement*, vol. 70, pp. 1–12, 2020.
- [27] A. Lou, S. Guan, H. Ko, and M. H. Loew, "Caranet: context axial reverse attention network for segmentation of small medical objects," in *Medical Imaging 2022: Image Processing*, vol. 12032. SPIE, 2022, pp. 81–92.
- [28] D.-P. Fan, G.-P. Ji, T. Zhou, G. Chen, H. Fu, J. Shen, and L. Shao, "Pranet: Parallel reverse attention network for polyp segmentation," in *International Conference on Medical Image Computing and Computer-Assisted Intervention*. Springer, 2020, pp. 263–273.
- [29] Z. Liu, Y. Lin, Y. Cao, H. Hu, Y. Wei, Z. Zhang, S. Lin, and B. Guo, "Swin transformer: Hierarchical vision transformer using shifted windows," in *Proceedings of the IEEE/CVF international conference on computer vision*, 2021, pp. 10012–10022.
- [30] E. Xie, W. Wang, Z. Yu, A. Anandkumar, J. M. Alvarez, and P. Luo, "Segformer: Simple and efficient design for semantic segmentation with transformers," *Advances in neural information processing systems*, vol. 34, pp. 12077–12090, 2021.
- [31] F. Shen, H. Ye, J. Zhang, C. Wang, X. Han, and Y. Wei, "Advancing pose-guided image synthesis with progressive conditional diffusion models," in *The Twelfth International Conference on Learning Representations*, 2023.
- [32] F. Shen, H. Ye, S. Liu, J. Zhang, C. Wang, X. Han, and W. Yang, "Boosting consistency in story visualization with rich-contextual conditional diffusion models," *arXiv preprint arXiv:2407.02482*, 2024.
- [33] F. Shen, X. Jiang, X. He, H. Ye, C. Wang, X. Du, Z. Li, and J. Tang, "Imagdressing-v1: Customizable virtual dressing," *arXiv preprint arXiv:2407.12705*, 2024.
- [34] F. Shen and J. Tang, "Imagpose: A unified conditional framework for pose-guided person generation," *Advances in neural information processing systems*, 2024.
- [35] Y. Zhang, H. Liu, and Q. Hu, "Transfuse: Fusing transformers and cnns for medical image segmentation," in *Medical image computing and computer assisted intervention—MICCAI 2021: 24th international conference, Strasbourg, France, September 27–October 1, 2021, proceedings, Part I 24*. Springer, 2021, pp. 14–24.
- [36] B. Dong, W. Wang, D.-P. Fan, J. Li, H. Fu, and L. Shao, "Polyp-pvt: Polyp segmentation with pyramid vision transformers," *arXiv preprint arXiv:2108.06932*, 2021.
- [37] N. T. Duc, N. T. Oanh, N. T. Thuy, T. M. Triet, and V. S. Dinh, "Colonformer: An efficient transformer based method for colon polyp segmentation," *IEEE Access*, vol. 10, pp. 80575–80586, 2022.
- [38] F. Tang, Z. Xu, Q. Huang, J. Wang, X. Hou, J. Su, and J. Liu, "Duat: Dual-aggregation transformer network for medical image segmentation," in *Chinese Conference on Pattern Recognition and Computer Vision (PRCV)*. Springer, 2023, pp. 343–356.
- [39] J. Wei, Y. Hu, R. Zhang, Z. Li, S. K. Zhou, and S. Cui, "Shallow attention network for polyp segmentation," in *Medical Image Computing and Computer Assisted Intervention—MICCAI 2021: 24th International Conference, Strasbourg, France, September 27–October 1, 2021, Proceedings, Part I 24*. Springer, 2021, pp. 699–708.
- [40] J. Wang, Q. Huang, F. Tang, J. Meng, J. Su, and S. Song, "Stepwise feature fusion: Local guides global," in *International Conference on Medical Image Computing and Computer-Assisted Intervention*. Springer, 2022, pp. 110–120.
- [41] W. Wang, E. Xie, X. Li, D.-P. Fan, K. Song, D. Liang, T. Lu, P. Luo, and L. Shao, "Pvt v2: Improved baselines with pyramid vision transformer," *Computational Visual Media*, vol. 8, no. 3, pp. 415–424, 2022.
- [42] I. Loshchilov and F. Hutter, "Decoupled weight decay regularization," *arXiv preprint arXiv:1711.05101*, 2017.

JINGJING REN received her bachelor's degree in electronic science and technology from Shanxi Normal University in 2007 and Master's degree in signal and information processing from Chongqing University in 2010. She is currently a lecturer. Her research interests include target detection and image segmentation.

XIAOYONG ZHANG received his M.S. degree in Signal and Information Processing and his Ph.D. degree in Instrumentation Science and Technology from North Central University in 2010 and 2021, respectively. He is currently an associate professor in the Department of Intelligence and Information Engineering at Taiyuan College. His research interests include embedded signal processing, machine learning, and their applications.

LINA ZHANG. received her bachelor's degree in computer science and technology from Northwestern Polytechnical University in 2006 and Master's degree in computer application technology from Taiyuan University of Technology in 2010. She is currently a lecturer. Her research interests include data analysis and target detection.

...